Clinical Neurophysiology 126 (2015) 2132–2141

Contents lists available at ScienceDirect

Clinical Neurophysiology

journal homepage: www.elsevier.com/locate/clinph

Identifying patients with Alzheimer's disease using resting-state fMRI and graph theory

Ali Khazaee [a,*], Ata Ebrahimzadeh [a], Abbas Babajani-Feremi [b,c]

[a] Department of Electrical and Computer Engineering, Babol University of Technology, Iran
[b] Department of Pediatrics, Division of Clinical Neurosciences, University of Tennessee Health Science Center, Memphis, TN, USA
[c] Neuroscience Institute, Le Bonheur Children's Hospital, Memphis, TN, USA

See Editorial, pages 2043–2044

ARTICLE INFO

Article history:
Accepted 3 February 2015
Available online 1 April 2015

Keywords:
Resting-state functional magnetic resonance imaging (rs-fMRI)
Alzheimer's disease (AD)
Graph theory
Machine learning
Statistical analysis

HIGHLIGHTS

- Resting-state fMRI data were used to classify healthy subjects and patients with AD.
- Brain network-based features were extracted.
- We were able to accurately classify AD from Normal with accuracy of 100%.

ABSTRACT

Objective: Study of brain network on the basis of resting-state functional magnetic resonance imaging (fMRI) has provided promising results to investigate changes in connectivity among different brain regions because of diseases. Graph theory can efficiently characterize different aspects of the brain network by calculating measures of integration and segregation.
Method: In this study, we combine graph theoretical approaches with advanced machine learning methods to study functional brain network alteration in patients with Alzheimer's disease (AD). Support vector machine (SVM) was used to explore the ability of graph measures in diagnosis of AD. We applied our method on the resting-state fMRI data of twenty patients with AD and twenty age and gender matched healthy subjects. The data were preprocessed and each subject's graph was constructed by parcellation of the whole brain into 90 distinct regions using the automated anatomical labeling (AAL) atlas. The graph measures were then calculated and used as the discriminating features. Extracted network-based features were fed to different feature selection algorithms to choose most significant features. In addition to the machine learning approach, statistical analysis was performed on connectivity matrices to find altered connectivity patterns in patients with AD.
Results: Using the selected features, we were able to accurately classify patients with AD from healthy subjects with accuracy of 100%.
Conclusion: Results of this study show that pattern recognition and graph of brain network, on the basis of the resting state fMRI data, can efficiently assist in the diagnosis of AD.
Significance: Classification based on the resting-state fMRI can be used as a non-invasive and automatic tool to diagnosis of Alzheimer's disease.

1. Introduction

Alzheimer's disease (AD) is the most common type of dementia (60–80% of cases) among older people (Reitz et al., 2011). The neuropathological hallmarks of AD are the accumulation of amyloid-β plaques and tau-related neurofibrillary tangles (Blennow et al., 2006; Holtzman et al., 2011). Resting-state functional magnetic

* Corresponding author at: Department of Electrical and Computer Engineering, Babol University of Technology, Shariati blvd., Babol, Iran. Tel.: +9811132310982.
E-mail address: khazaeeali@yahoo.com (A. Khazaee).

http://dx.doi.org/10.1016/j.clinph.2015.02.060
1388-2457/

resonance imaging (rs-fMRI) is a non-invasive method that has been used for detection of AD. Resting-state fMRI is on the basis of the spontaneous low frequency fluctuations (<0.1 Hz) in the blood oxygen level-dependent (BOLD) signal (Biswal et al., 1995). Resting-state networks (RSNs) are determined by investigating synchronous activations of the BOLD signal between distinct brain regions (Lee et al., 2013). Various brain diseases may influence RSNs. The default-mode network, first identified by Raichle et al. (2001), was implicated in AD pathophysiology (Greicius et al., 2004; Koch et al., 2012).

Automatic diagnosis of brain diseases using rs-fMRI have been investigated by several studies in recent years (Chen et al., 2011; Brier et al., 2012; Liu et al., 2015; Tang et al., 2013; Hoekzema et al., 2014; Zeng et al., 2014). A common methodology for classification of patients with AD (Chen et al., 2011), attention deficit hyperactivity (ADHD) (Hoekzema et al., 2014), major depression (Zeng et al., 2014), social anxiety disorder (Liu et al., 2015), and antisocial personality disorder (Tang et al., 2013) from the normal subjects, was to use a large number of correlation coefficients of pairwise regions of interests (ROIs). Another methodology for identifying patients from normal subjects was to use averaged pairwise correlation as a data reduction strategy (Brier et al., 2012). However, these methodologies were not efficient in classification of the patients from the normal subjects since the dynamics of the whole-brain network was ignored in these studies. Because the brain is a highly complex system (Passingham et al., 2002; Sporns et al., 2005), revealing the mechanism of brain diseases by studying only the rs-fMRI correlation between different areas of the brain may not be efficient. A more sophisticated analysis of the brain intrinsic activity is needed. The properties of complex systems can be quantified adequately by using graph theory. Graph theory models interrelationships (represented by edges) between brain regions (represented by nodes) and assess the state of the brain network using various measures (Bullmore and Sporns, 2009). It has been shown in various studies that graph theory is sensitive in identifying network measures of psychiatric and neurological diseases (Bassett et al., 2008; Bassett and Bullmore, 2009; Lynall et al., 2010; van den Heuvel et al., 2010; Wang et al., 2010; Zhang et al., 2011).

Despite the great success of machine learning in diagnosis of disease, automatic classification of AD from normal subjects using rs-fMRI data has received little attention from the neuroimaging researchers (Wang et al., 2006a; Chen et al., 2011; Dai et al., 2012; Zhang et al., 2012; Li et al., 2013). Furthermore, these studies have used limited discriminant features such as correlation coefficients between specific brain regions (Wang et al., 2006a; Chen et al., 2011), regional homogeneity (ReHo), and amplitude of low-frequency fluctuations (ALFF) (Dai et al., 2012; Zhang et al., 2012). In another study, a limited number of brain network measures was employed as discriminative features (Li et al., 2013). However, these studies have not achieved a good performance because the utilized features in these studies only consider specific local properties and ignore dynamics of the whole-brain.

The main contribution of the current study is to propose an automated and accurate method for classification of patients with AD from healthy subjects. We performed a significance analysis to find significant correlations in healthy control subjects and patients with AD. Then we compared these correlations to find the alterations in functional connectivity of brain regions during AD. The classification method used in this study consisted of four modules, namely, preprocessing, feature extraction, feature selection and classification. The feature extraction module, is based on a diverse set of segregation, integration, and local brain network measures. Another novelty of our study is related to the feature selection module which selects the most relevant and informative feature of an original feature set and improves the accuracy of the final classification. Several feature selection algorithms have been investigated and the best one selected for subsequent analysis. Each algorithm sorts the original feature set according to its discrimination ability. In the classification module, we have used the support vector machine (SVM) as the learning algorithm. The SVM has been received a lot of attention in bioinformatics applications, due to the its accuracy, ability to handle high-dimensional data, and flexibility in modeling diverse sources of data (Schölkopf et al., 2004; Noble, 2006). We hypothesized that the proposed approach in the current study can accurately discriminate healthy subjects from patients with AD. In addition, the selected features in feature selection module and the statistical analysis provide information about functional alteration due to the AD.

2. Methods

2.1. Subjects

Twenty patients with AD (average age 74.9 years, 10 female) and twenty age-matched healthy controls (average age 75.1 years, 10 female) from the Alzheimer's disease neuroimaging initiative (ADNI) database (http://adni.loni.ucla.edu) were analyzed in this study. Data for this study were selected based on availability of resting-state fMRI datasets for age-matched healthy normal subjects and patients with AD. The patients with AD had a Mini-Mental State Examination (MMSE) score of 14–26 and a Clinical Dementia Rating (CDR) of 0.5 or 1.0 and met the National Institute of Neurological and Communicative Disorders and Stroke and the Alzheimer's Disease and Related Disorders Association (NINCDS/ADRDA) criteria for probable AD. The normal subjects were non-depressed, non-MCI, and non-demented and had a MMSE score of 27–30 and a CDR of 0. Demographic information of subjects is summarized in Table 1.

2.2. Data acquisition and preprocessing

Resting fMRI data and structural MRI scans were acquired with 3.0 T Philips scanners. Acquisitions were performed according to the ADNI acquisition protocol (Jack et al., 2008). Resting state scans consisted of 140 functional volumes (TR/TE 3000/30 ms, flip angle = 80°, 3.313 mm slice thickness, 48 slices). To allow the participant's adaptation to the circumstances and for signal equilibrium, the first few volumes (7 volumes) of the functional images of each subject were discarded. Image preprocessing was carried out using the Data Processing Assistant for Resting-State fMRI (DPARSF) toolbox and the SPM5 package (http://www.fil.ion.ucl.ac.uk/spm) (Chao-Gan and Yu-Feng, 2010).

Resting-state fMRI scans were gone under standard pre-processing steps. Slice-time correction for interleaved acquisition was performed. Motion correction was performed by realigning fMRI time-series using a six-parameter rigid-body spatial transformation (Friston et al., 1995). In this study, all subjects had less

Table 1
Demographic of healthy control subjects and patients with AD.

	Healthy control	Patients with AD
Number	20	20
Male/female	10/10	10/10
Age*	75.0512 ± 4.9239	74.8553 ± 4.5035
MMSE score^	29.4375 ± 0.8638	20.8947 ± 3.4473
CDR score+	0.0333 ± 0.1247	0.9211 ± 0.3349

* p-Value = 0.8989 (two-sample t-test).
^ p-Value = 7.8355e−11 (two-sample t-test); four control subjects and one patient with AD did not have MMSE score.
+ p-Value = 8.7875e−11 (two-sample t-test); five control subjects and one patient with AD did not have CDR score.

than 2.5 mm of displacement and 2.5° of rotation in any direction. Thus, no participant was excluded. Normalization into the Montreal Neurological Institute (MNI) space was performed using echo-planar imaging (EPI) template (Ashburner and Friston, 1999) and then all images resampled to 3-mm isotropic voxels. Then, detrending and spatial smoothing using a Gaussian kernel of FWHM = 4 mm were performed. The resulted images were then band-pass filtered (0.01–0.08 Hz) to retain low frequency fluctuations of the resting-state fMRI which have been suggested to reflect spontaneous neuronal activity (Lu et al., 2007). Higher frequencies originate from white matter and other physiological noises such as respiratory and cardiac signals. To reduce the effect of the physiological artifacts, the whole-brain signal was removed by a multiple linear regression analysis (Greicius et al., 2003; Fox et al., 2005; Fransson, 2005). In addition to the global mean signal, six head motion parameters, the cerebrospinal fluid (CSF), and the white matter signals were also removed as nuisance covariates to reduce the effects of motion and non-neuronal BOLD fluctuations (Fox et al., 2005; Kelly et al., 2008).

2.3. Brain network analysis

The nodes of the brain network were defined by parcellation of the whole brain into 90 distinct regions using the automated anatomical labeling (AAL) atlas (Tzourio-Mazoyer et al., 2002). The time series of voxels within each region was averaged and the resulted signal was used as the representative signal of the node. Pearson's correlation coefficients of signals of all pairs of AAL regions were employed to define the edges of the brain network. The resulted functional connectivity network has 4005 weighted edges and thus is a dense network. The connectivity matrix were thresholded by preserving a proportion P ($0 < P < 1$) of the strongest weights. All diagonal weights (self-connections) were set to zero. There is not a straightforward rule for finding the threshold value. We performed a search over different thresholds to find the optimal threshold value. A high value of P keeps more graph edges which corresponds to noisy and less significant correlations and results in a denser network. On the other hand, setting a small value to P removes many edges from the graph and generates a disconnected graph in which the graph metrics may not be calculated.

2.4. Computation of graph metrics

To produce efficient features, different graph metrics were computed. Three measures of functional segregation (clustering coefficient, local efficiency, and normalized local efficiency), two functional integration measures (characteristic path length and global efficiency), three local nodal measures (degree, participation coefficient, and betweenness centrality), and one measure of network small-worldness were computed. Functional segregation measures characterize the ability of the brain for specialized processing to occur within densely interconnected groups of regions while the functional integration measures assess ability of the brain in rapidly combining specialized information from distributed regions. The graph measures were calculated based on the weighted adjacency matrices using the Brain Connectivity Toolbox (www.brain-connectivity-toolbox.net) (Rubinov and Sporns, 2010). A brief description of the calculated measures is as follows.

2.4.1. Measures of functional segregation

The binary clustering coefficient of a particular node is the proportion of the number of edges that exists between neighbors of that node relative to the number of all possible edges between neighbors. The weighted clustering coefficient is a generalized version of binary clustering coefficient and incorporates the weights of the edges in the definition (Watts and Strogatz, 1998; Barrat et al., 2004; Onnela et al., 2005). The overall clustering coefficient in a network, which is indicative of the presence of clustered connectivity around individual nodes ("cliques"), can be calculated by averaging the clustering coefficient across all individual nodes. The ability of a network in transmitting information at the local level can be determined by measure of local efficiency (Latora and Marchiori, 2001; Onnela et al., 2005; Rubinov and Sporns, 2010). Ratio of local efficiency to the global efficiency was calculated as a separate measure, namely, normalized local efficiency.

2.4.2. Measures of functional integration

The most frequently used measure of functional integration is characteristic path length. Characteristic path length of a network is defined as the mean of the shortest geodesic distances between all possible pairs of nodes (average shortest distance between any two nodes) in the network (Watts and Strogatz, 1998). Path length for a weighted graph is calculated as the total sum of inverse weights of individual edges. Global efficiency measures the ability of a network to transmit information at the global level and is defined as the average inverse shortest path length (Latora and Marchiori, 2001).

2.4.3. Regional nodal measures

The properties of brain regions can be measured through the centrality of individual nodes in the brain network. The simplest measure of centrality is the degree of node and for a weighted undirected network is defined as the sum of weights of edges connected to a node. The degree has a straightforward implication. A node with a high value of degree means that there is more interaction between the node and many other nodes, and consequently it is an important node in the network. The network's modular structure is determined by maximizing the value of modularity. The modularity of a network is defined as the ratio of the number of within groups edges to the number of between groups edges (Blondel et al., 2008; Rubinov and Sporns, 2011). Once the network modules are revealed, the diversity of inter-module connections of nodes can be assessed by a measure known as the participation coefficient (Guimera and Amaral, 2005; Guimera et al., 2007). Nodes with a high participation coefficient maintain a diverse set of inter-modular connections and are known as connector hubs. Hub nodes are likely to facilitate between-module integration. High-degree nodes with a low participation coefficient are called provincial hubs and mostly participate in within-module interactions. Betweenness centrality is a common measure of centrality and is based on the concept of shortest paths. The betweenness centrality of a particular node is equal to the number of shortest paths from all nodes to all others that pass through that node (Freeman, 1979; Brandes, 2001). A weighted variant of betweenness centrality is calculated using weighted variants of degree and path length.

It has been shown in various studies that the brain network is organized according to an efficient small-world organization (Watts and Strogatz, 1998; Humphries and Gurney, 2008). A common finding is that small-world organization reflects an optimal balance of functional integration and segregation (Sporns and Honey, 2006). Small-world networks are highly clustered like regular networks yet have small characteristic path lengths like random graphs. Humphries and colleagues introduced the measure of small-worldness as a ratio of network clustering coefficient and characteristic path length compared to their corresponding random network values (Humphries and Gurney, 2008).

The calculated measures, together, construct the final feature vector for each subject. Each local network measure (i.e. degree, participation coefficient, betweenness centrality, local efficiency, ratio of local to global efficiency) provides 90 feature values (because

the number of nodes in this study was 90) and each global network measure (i.e. average path length, average clustering coefficient, global efficiency, and small-worldness) provides one feature value. Thus, the size of the final feature vector was 454; 90 regions × 5 (nodal network measures) + 4 global network measures.

As explained in Section 2.3, graphs were thresholded to eliminate statistically insignificant correlations. Some thresholded graphs may have disconnected nodes which influence the calculation of graph measures. To overcome this problem, the bridging edges between disconnected nodes were retained, irrespective of the weight of the edge.

2.5. Feature selection and classification

Feature selection module selects an optimal subset of features from the original feature set and is a required stage in the case of high dimensional data (such as fMRI). We examined seven different feature selection methods and selected the Fisher score feature selection algorithm. Fisher score is a univariate feature selection algorithm that is independent of the class distribution and is commonly employed to determine the discriminatory power of individual features between two classes of equal probability (Duda et al., 2012). Fisher score for each feature in a two class problem is defined as:

$$\mathrm{FS} = \frac{n_1(m_1 - m)^2 + n_2(m_2 - m)^2}{(n_1\sigma_1^2 + n_2\sigma_2^2)} \quad (1)$$

where m is the mean of the feature, m_1 and m_2 are feature mean values on each class, σ_1^2 and σ_2^2 are respective variances, and n_1 and n_2 are number of samples in the classes.

After the feature selection stage, supervised machine learning methods were used to construct the classifier. The supervised machine learning algorithm was trained using a set of input data to produce the desired output. The supervised machine learning algorithm used in this study was the support vector machine (SVM) (Noble, 2006). The SVM was implemented in MATLAB (The Math Works, Natwick, MA) and LIBSVM (http://www.csie.ntu.edu.tw/~cjlin/libsvm/).

Data acquisition in human neuroimaging studies is costly and therefore the number of available subjects is small. The small number of training and test samples can cause the generalization ability of the study. Thus, employing cross-validation strategies is inevitable. One of the frequently used methods in such situations is leave-one-out cross-validation (LOOCV). LOOCV is repeated N times (N is the number of all subjects, here is 40) and in every iteration one sample is leaved out to test the classifier and remaining subjects are fed to classifier for training. The procedure is repeated until all subjects used once as test sample. Finally, the result for every repetition is averaged to produce the final classification accuracy (Fig. 1).

3. Results

We performed two kinds of analysis based on the brain network graph. Firstly, a *statistical analysis* was performed to find statistically significant edges in healthy control group and patients with AD. Secondly, a *machine learning based analysis* was performed. The graphs were thresholded and graph measures were calculated for classification of patients with AD from healthy control subjects. In *statistical analysis*, a p-value was assigned to each of the edges. All p-values were corrected for multiple testing using the false discovery rate (FDR) method (Benjamini et al., 1995). To assign p-values, a surrogate data method was used (Theiler et al., 1992). The method selects the most significant values of the graph at the 99% confidence level. For fMRI signals of each node, 200 surrogates were generated by randomizing the signals. Significant edges were selected such that the expected fraction of false positives was restricted to $q \leqslant 0.01$ (Dimitriadis et al., 2012). This procedure was repeated for all subjects and found the significant edges of each subject. We compared the significant edges of subjects of each group (Normal and AD) and selected edges that was significant in all subjects of the group. Table 2 and Fig. 2 show the results. In *machine learning based analysis*, the graphs should be sparse through thresholding. A search-based method was proposed to convert fully connected functional brain networks to sparse brain networks. The method searches over the proportional threshold values in the range [0.05–0.7] with an increment step of 0.01. In each threshold value, the graph was thresholded and then, all of the stages including feature extraction, feature selection and LOOCV classification were performed. According to the Fig. 3, the proportional threshold value of 0.19 (i.e. preserving 19% of the strongest weights) achieved the best classification performance. Therefore, this threshold value was selected for further analysis. The topology and connection matrix of the fully connected and sparse brain network are shown in Fig. 4.

After the feature extraction stage, a feature vector with a size of 454 for each subject (normal or AD) was generated. Because of the high dimensionality of the feature data, various feature selection algorithms were compared to reduce the complexity of the classification problem and Fisher score algorithm were selected. The Fisher algorithm provides a sorted features list according to its discrimination ability. The best feature is on the top of the list with maximum discrimination. We first trained and tested the classifier using the best feature and obtained the corresponding classification accuracy. Then we trained and tested the classifier using the best two features and obtained the classification accuracy. The number of used features increased in each step of the experiment until all of features used to train and test the classifier were included. Classification accuracy reaches its maximum value at a certain number of features. The number of features that resulted in the best performance was 21. Fig. 5 shows the type of selected measures and Table 3 shows the mean and standard deviation of their values for both normal and AD groups. These measures were related to the specific nodes. According to the Fisher score algorithm, 16 different nodes had most differentiation between Normal and AD groups, which four nodes were associated to more than one measure (Table 4). Left caudate nucleus (CAU.L) were associated to three measures and orbital part of the left inferior frontal gyrus (ORBinf.L), dorsolateral of the left superior frontal gyrus (SFGdor.L), and opercular part of the right inferior frontal gyrus (IFGoperc.R) were associated to two measures. These nodes are marked with green color in Fig. 6 and other AAL nodes are shown in red.

A popular assessment of the AD severity is the MMSE score. To estimate the association between AD disease severity and discriminative parameters, we calculated the correlation between MMSE score of patients with AD and nodal network measures. Table 5 shows the results. Finally, we have compared performance of classification using some popular classifiers in neuroimaging studies, including, linear SVM, Gaussian radial basis function (GRBF) SVM, polynomial SVM, and k-nearest neighbor classifier (KNN). Results are shown in Table 6.

4. Discussions

In this study, we analyzed the brain network to find significant alterations due to the AD. In addition, we investigated whether graph theoretical measures derived from the brain complex network are able to accurately discriminate between patients with AD and healthy control subjects. Using the correlation between resting-state fMRI signals of brain regions, the functional network of the brain was constructed. As shown in Table 2 and Fig. 2 and 11

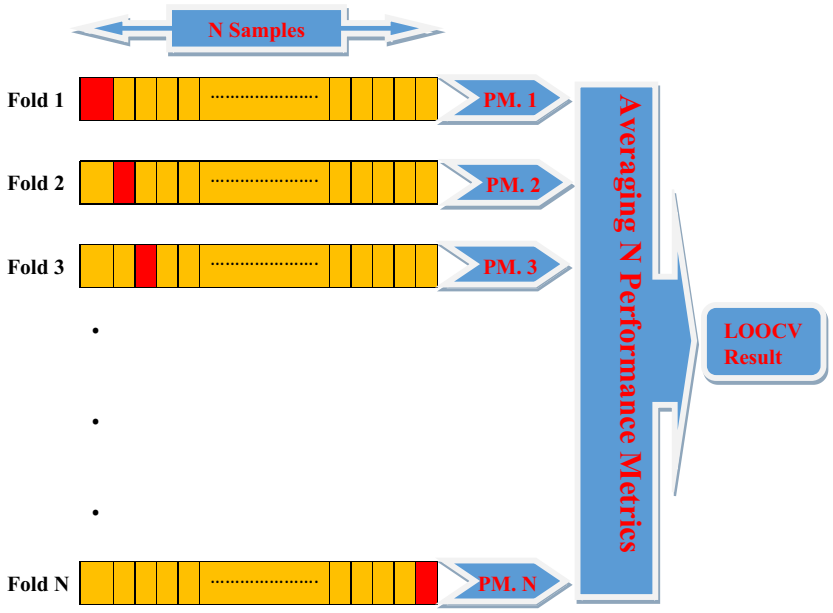

Fig. 1. Schematic view of leave-one-out cross-validation (LOOCV) algorithm. Samples colored as yellow are the training sets and the red sample is the one that leaved out for test. PM: performance metric. (For interpretation of the references to color in this figure legend, the reader is referred to the web version of this article.)

Table 2
Significant edges (correlations) of the brain network in normal subjects and patients with AD. Significant edges which there are not in both groups were printed in bold font.

Significant edges in healthy control subjects		Significant edges in patients with AD	
Region 1	Region 2	Region 1	Region 2
OLF.L	OLF.R	**SFGdor.L**	**MFG.L**
SFGdor.L	SFGmed.L	**SFGdor.R**	**MFG.R**
SFGmed.L	SFGmed.R	**ORBsup.L**	**ORBmid.L**
REC.L	**REC.R**	**SMA.L**	**SMA.R**
ACG.L	**ACG.R**	OLF.L	OLF.R
DCG.L	DCG.R	SFGdor.L	SFGmed.L
PCG.L	PCG.R	SFGmed.L	SFGmed.R
CAL.L	CAL.R	**ORBsupmed.L**	**ORBsupmed.R**
CUN.L	CUN.R	**ROL.R**	**INS.R**
SOG.L	MOG.L	DCG.L	DCG.R
PreCG.R	PoCG.R	PCG.L	PCG.R
SPG.L	IPL.L	CAL.L	CAL.R
PCUN.L	PCUN.R	CUN.L	CUN.R
PUT.L	**PUT.R**	**CAL.L**	**LING.L**
THA.L	**THA.R**	**CAL.R**	**LING.L**
		CAL.R	**LING.R**
		LING.L	**LING.R**
		CUN.R	**SOG.R**
		SOG.L	MOG.L
		SOG.R	**MOG.R**
		MOG.R	**IOG.R**
		PreCG.L	**PoCG.L**
		PreCG.R	PoCG.R
		SPG.L	IPL.L
		PCUN.L	PCUN.R
		PUT.L	**PAL.L**
		TPOmid.L	**TPOmid.R**

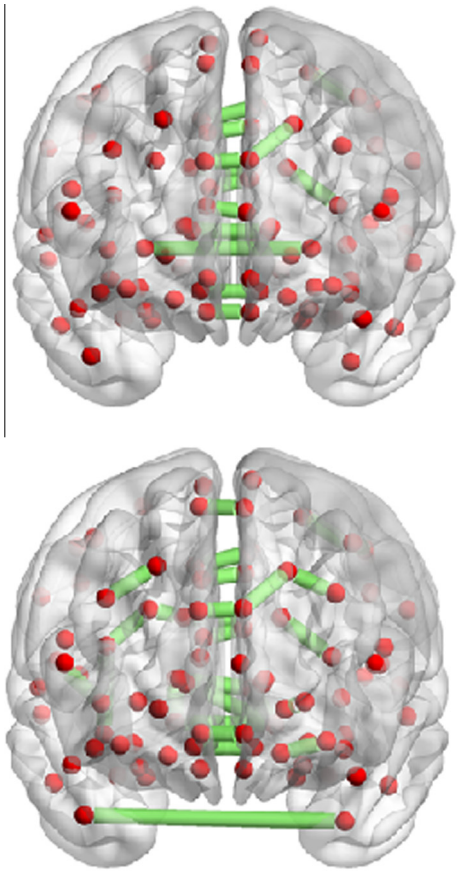

Fig. 2. Coronal view of the significant edges (correlations) of the brain network in normal subjects (top) and patients with AD (bottom).

significant edges are the same in both normal and AD subjects. There are 4 significant edges (correlations) in normal subjects which are turned to insignificant edges in AD subjects (bolded regions in the left column of Table 2). This may suggest a weaker interregional correlation between left and right lobes of gyrus rectus, anterior cingulate and paracingulate gyri, putamen of the lenticular nucleus, and thalamus in patients with AD. On the other hand, there are 16 significant edges in patients with AD which were insignificant in normal subjects (bolded regions in the right column of Table 2). Most of these edges are distributed within a limited area of each brain lobe. Our results support the resting-state fMRI studies which reported increased interregional functional connectivity within each brain lobe and decreased interregional functional connectivity between brain lobes in AD (Wang

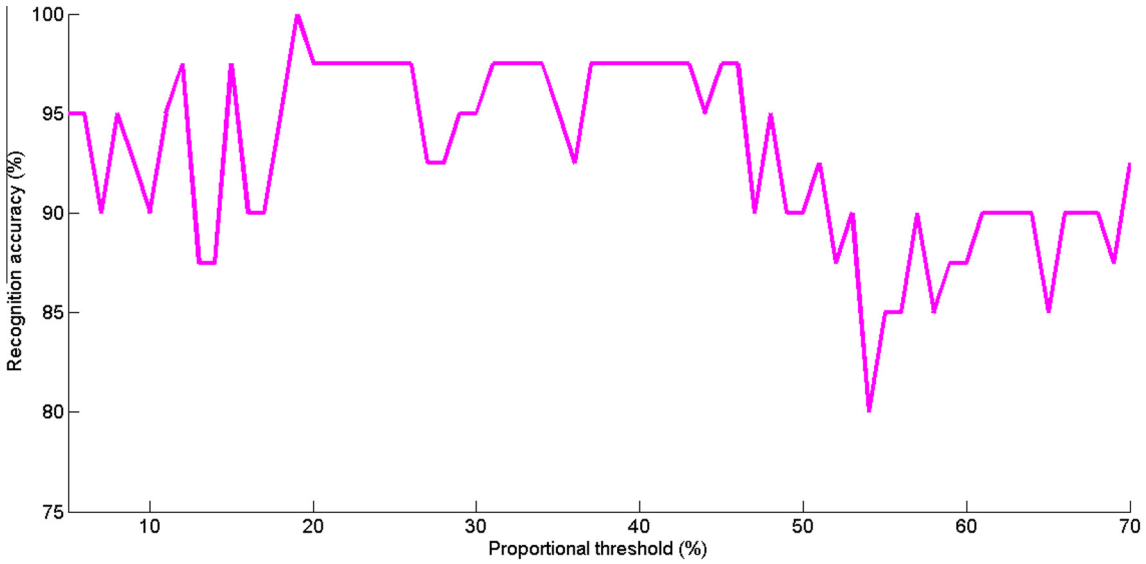

Fig. 3. Performance of classification in different values of proportional threshold.

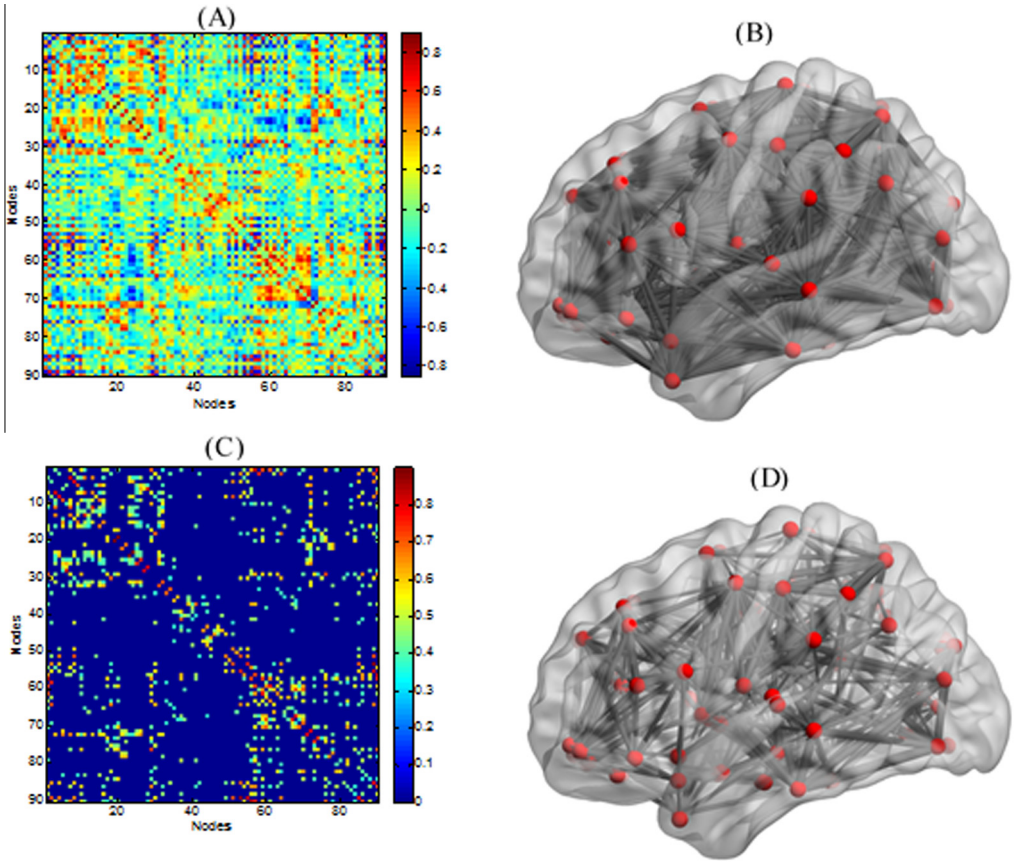

Fig. 4. Topology and functional connectivity network. The connectivity matrix (A) and topology (B) of the fully connected network of a representative normal subject are shown. (C) and (D) are same as (A) and (B) except only 19% of edges are retained. Plots of this figure were created using the BrainNet Viewer software package (http://nitrc.org/projects/bnv/).

et al., 2007). In addition, we observed great alteration in lingual gyrus in patients with AD. According to Table 2, there are significant correlation between left and right lingual gyrus (LING.L and LING.R), lingual gyrus and right calcarine fissure and surrounding cortex (CAL.R and LING.R, CAL.R and LING.L), and left lingual gyrus and left calcarine fissure and surrounding cortex (CAL.L and LING.L). Another important observation is related to the significant correlations of occipital gyrus in patients with AD. There are significant correlations between right middle occipital gyrus and right inferior occipital gyrus (MOG.R and IOG.R), right superior occipital gyrus and right middle occipital gyrus (SOG.R and MOG.R), and right cuneus and right superior occipital gyrus (CUN.R and SOG.R). Superior frontal gyrus is another region which has significant correlations in patients with AD. These correlations are between dorsolateral of the left superior frontal gyrus and left middle frontal gyrus (SFGdor.L and MFG.L), dorsolateral of the right

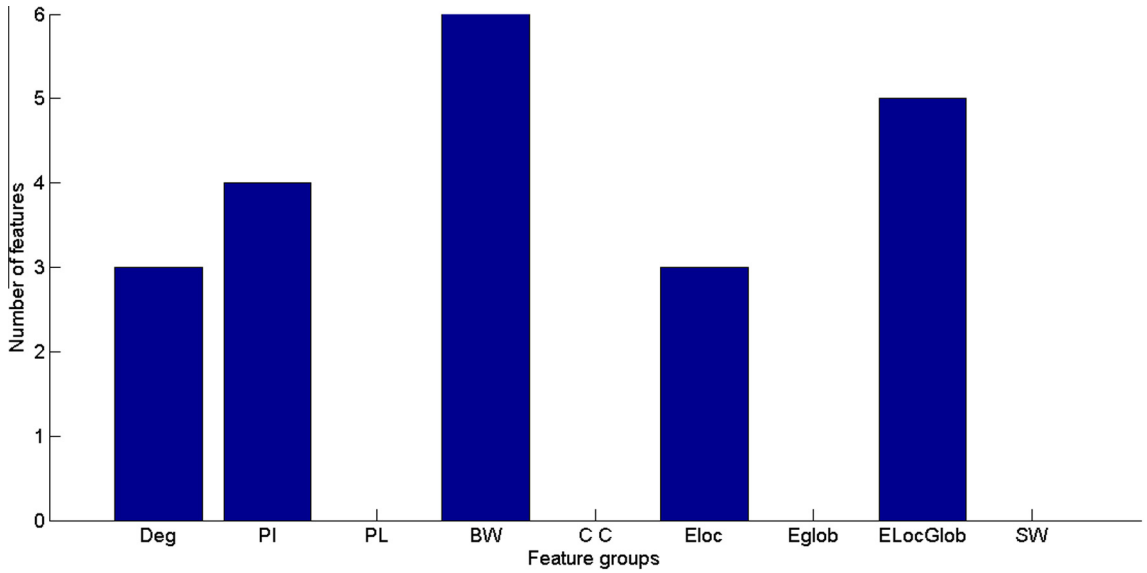

Fig. 5. Number of the selected features from each group by the Fisher algorithm. Deg: degree; PI: participation coefficient; PL: average characteristic path length; BW: betweenness centrality; CC: average clustering coefficient; Eloc: local efficiency; Eglob: global efficiency; ELocGlob: ratio of local to global efficiency; SW: small-world index.

Table 3
The values of average and standard deviation of selected measures in healthy control and patients with AD.

Selected measures	Healthy control (mean ± standard deviation)	Patients with AD (mean ± standard deviation)
Participation coefficient of CAL.L	44.45 ± 20.0237	21.35 ± 21.0625
Betweenness centrality of ORBinf.L	79.7 ± 52.8783	183 ± 125.1135
Normalized local efficiency of IFGoperc.R	1.6574 ± 0.1415	1.5217 ± 0.1387
Normalized local efficiency of SFGdor.L	1.6578 ± 0.1797	1.8759 ± 0.2646
Betweenness centrality of MFG.L	96.7 ± 85.2626	179.7 ± 94.7022
Betweenness centrality of MTG.L	168.4 ± 115.0662	78.4 ± 77.3320
Participation coefficient of PCG.R	23.7 ± 16.2453	42.65 ± 24.2967
Local efficiency of IFGoperc.R	0.3928 ± 0.0499	0.3556 ± 0.0351
Normalized local efficiency of CAU.L	1.3534 ± 0.4138	1.6168 ± 0.1717
Degree of CAU.L	14.95 ± 5.6787	20.2 ± 7.0470
Participation coefficient of LING.R	43.9 ± 24.5375	25 ± 22.4789
Normalized local efficiency of ORBmid.L	1.6327 ± 0.3188	1.8810 ± 0.3003
Degree of ORBinf.L	16.05 ± 6.0949	20.8 ± 6.1041
Betweenness centrality of INS.R	113.8 ± 77.5446	198.5 ± 134.6371
Betweenness centrality of SFGmed.R	137.7 ± 86.2793	79.6 ± 63.2759
Degree of MTG.R	17.6 ± 5.9867	13.1 ± 6.2682
Normalized local efficiency of SFGdor.R	1.6935 ± 0.2678	1.8835 ± 0.2552
Local efficiency of SFGdor.L	0.3927 ± 0.0556	0.4400 ± 0.0747
Participation coefficient of OLF.R	62.95 ± 22.7519	76.2 ± 12.9484
Local efficiency of CAU.L	0.3209 ± 0.1064	0.3789 ± 0.0507
Betweenness centrality of SMG.R	174.9 ± 128.4780	101.20 ± 82.3442

Table 4
The AAL regions that show highest discrimination ability.

Name of the AAL region	Abbreviation
Dorsolateral of the left superior frontal gyrus	SFGdor.L
Dorsolateral of the right superior frontal gyrus	SFGdor.R
Left middle frontal gyrus	MFG.L
Orbital part of the left middle frontal gyrus	ORBmid.L
Opercular part of the right inferior frontal gyrus	IFGoperc.R
Orbital part of the left inferior frontal gyrus	ORBinf.L
Right olfactory cortex	OLF.R
Right medial superior frontal gyrus,	SFGmed.R
Right insula	INS.R
Right posterior cingulate gyrus	PCG.R
Left calcarine fissure and surrounding cortex	CAL.L
Right lingual gyrus	LING.R
Right supramarginal gyrus	SMG.R
Left caudate nucleus	CAU.L
Left middle temporal gyrus	MTG.L
Right middle temporal gyrus	MTG.R

superior frontal gyrus and right middle frontal gyrus (SFGdor.R and MFG.R), orbital part of the left superior frontal gyrus and orbital part of the left middle frontal gyrus (ORBsup.L and ORBmid.L), and medial orbital of the left superior frontal gyrus and medial orbital of the right superior frontal gyrus (ORBsupmed.L and ORBsupmed.R). These results are consistent with previous studies which reported significant changes in the middle occipital gyrus (Smith et al., 2009), inferior occipital gyrus (Melrose et al., 2009), lingual gyrus (Eustache et al., 2004), and superior frontal gyrus (Desgranges et al., 2002). After statistical analysis of functional connectivity in the brain, we hypothesized to use brain network measures as discriminative features for automatically classifying patients with AD from healthy control subjects. To do this task, we constructed sparse brain network by thresholding complex brain network. As shown in Fig. 3, the best performance of classification were achieved in 0.19 proportional threshold where the LOOCV based classification accuracy was 100%. As it can be seen from Fig. 4, an appropriate thresholding reduces the complexity of the network while maintaining important edges. After thresholding, various measures of graph segregation and integration were extracted and fed to the SVM classifier as discriminative features. Feature selection methods were employed to select the most efficient features.

Overall, the main advantage of feature selection is not to improve performance of the classifier rather is to obtain better understanding of data. Different feature selection algorithms

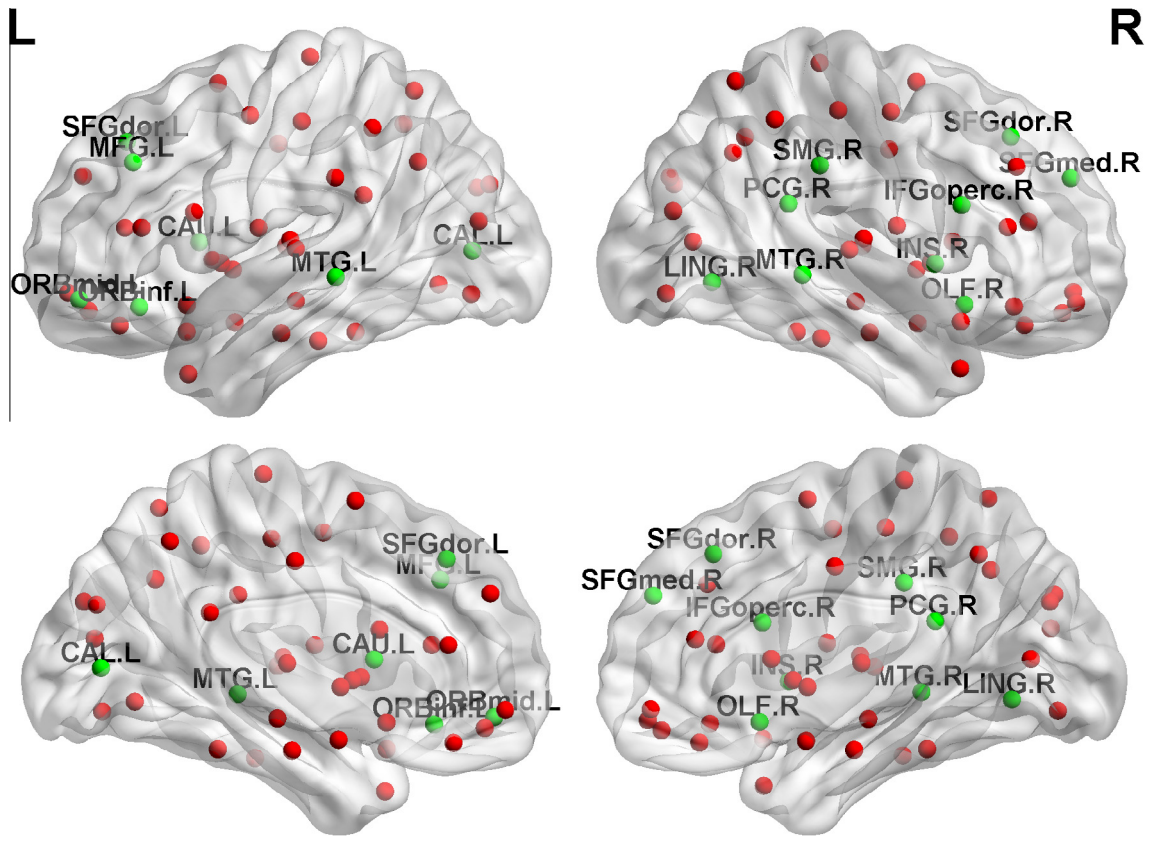

Fig. 6. Location of the areas in the AAL atlas that show highest discrimination ability. Circles represent AAL nodes and green nodes are those with higher discrimination ability between normal and AD groups. (For interpretation of the references to color in this figure legend, the reader is referred to the web version of this article.)

Table 5
Estimation of correlation between MMSE score of patients with AD and nodal network measures, i.e. degree, participation coefficient, betweenness centrality, and local efficiency. AAL regions with significant correlation were listed.

Graph measure	AAL Region	Correlation value	*P*-value
Participation coefficient	Left cuneus	−0.5414	0.0167
Local efficiency	Opercular part of right inferior frontal gyrus	0.7070	0.0007
	Right olfactory cortex	0.4750	0.0398
Degree	Left Insula	0.5130	0.0247
	Right lingual gyrus	0.4659	0.0444
	Right superior occipital gyrus	−0.4885	0.0338
	Left precuneus	−0.5722	0.0105
	Right superior temporal gyrus	0.5075	0.0266
Betweenness centrality	Triangular part of right inferior frontal gyrus	−0.6549	0.0023
	Left Rolandic operculum	0.4777	0.0386
	Right posterior cingulate gyrus	0.4996	0.0294
	Left lingual gyrus	−0.4607	0.0471
	Left fusiform gyrus	0.5464	0.0155
	Right superior parietal gyrus	0.5742	0.0101
	Right temporal pole: superior temporal gyrus	−0.5067	0.0268

Table 6
Performance of different classifiers for classification of AD.

Classifier	Parameters	Accuracy (%)
SVM (linear)	$C = 100$	100
SVM (GRBF)	$C = 1$, gamma = 0.000001	90
SVM (polynomial)	$C = 10$, degree = 3	90
KNN	$K = 1$	87.5

facilitate finding information about why a classifier made a particular prediction. They do this task by reducing the set of features to a small salient set (Ben-Hur and Weston, 2010). Fig. 5 illustrates the most informative features that help classifier to make best prediction. Approximately, all groups contribute to the classifier performance. However, these measures are related to specific nodes in the brain that are the most influenced regions in AD pathology (Table 4 and Fig. 6).

More than one measure of the left caudate nucleus and three regions in frontal gyrus i.e. dorsolateral of the left superior frontal gyrus, Orbital part of the left Inferior frontal gyrus, and opercular part of the right inferior frontal gyrus contributed to the classification performance. In addition betweenness centrality of right insula was selected by feature selection algorithm. Using the voxel based morphometry (VBM) method, previous studies showed atrophy of the some localized regions in the temporal lobe, insular cortex, caudate nucleus, and frontal cortex (Frisoni et al., 2002; Busatto et al., 2003; Karas et al., 2004) in patients with AD. Recently, studies of functional and structural brain networks in AD patients have indicated that cognitive function deficits could be due to abnormalities in the connectivity between different brain areas such as the middle temporal gyrus (Stam et al., 2007; He et al., 2008). Consistently, in our study, left and right middle temporal gyrus was determined to be altered during AD (Table 4). In addition, voxel-based analysis studies demonstrate significant changes in the middle temporal gyrus (Busatto et al., 2003), and inferior frontal gyrus (Kim et al., 2011). Besides, PET studies showed significant abnormalities in the lingual gyrus (Eustache et al., 2004), superior frontal gyrus (Desgranges et al., 2002). These observations are confirmed by our results in Table 4. The fact that our results are consistent with the previous studies suggests the effectiveness of our

algorithm for AD analysis and classification. It has been shown that the posterior cingulate cortex (PCG) in the default mode network (DMN) has a high diagnostic power for detection of AD (Wang et al., 2006b; Sorg et al., 2007; Koch et al., 2012; Tijms et al., 2013). The participation coefficient (PI) of the PCG in our study was a discriminative feature that contributed significantly to the classification accuracy (Table 4 and Fig. 6). The significant difference ($p = 0.0075$, FDR-corrected) between the values of this feature in two classes is suggestive of a loss of hubs in patients with AD and is considered responsible for decreased metabolism in the PCG in early AD (Minoshima et al., 1997), typically observed in PET studies. Our results show that the rank of the clustering coefficient feature was 442 among all 454 features and this feature is unable to significantly differentiate patients with AD from control subjects ($p = 0.9738$, FDR-corrected). This result is consistent with previous studies (Stam et al., 2007; Lo et al., 2010; Sanz-Arigita et al., 2010).

As shown in Table 5, regions that showed maximum correlation with MMSE score were opercular part of the right inferior frontal gyrus, left insula, right superior parietal gyrus, and left angular gyrus. The regions that showed maximum anticorrelation with MMSE score were triangular part of the right inferior frontal gyrus, left cuneus, right angular gyrus, and left precuneus. Interestingly, these regions are previously reported as affected regions in AD, especially parietal gyrus and precuneus. In addition, there were overlaps between regions with the highest correlation coefficients with MMSE scores (Table 5) and regions that showed highest discrimination ability between healthy controls and patients with AD (Table 4 and Fig. 6), including right lingual gyrus, right posterior cingulate gyrus, right olfactory cortex, and opercular part of the right inferior frontal gyrus.

Model selection is one of the most important pitfalls in classification problems. The choice of SVM kernel is data dependent and several kernels should be examined. However, in bioinformatic applications, in which data are high-dimensional and the number of subjects is small, linear kernel often provides the best result (Ben-Hur and Weston, 2010). In such applications, the flexibility of the Gaussian and polynomial kernels usually leads to the overfitting and consequently poor results. Results in Table 6 confirm that. Another advantage of linear kernel is that the only hyperparameter that needs to be adjusted is C, a soft margin constant of SVM classifier.

The current study proposed an algorithm that can identify patients with AD with an accuracy of 100%. In addition, using statistical analysis of functional connectivity between the brain regions and based on the high discriminative features, we identified brain regions with maximum abnormal functionality in patients with AD. The obtained results was in good agreement with previously reported results. However, there are limitations that should be addresses in future studies. The obtained accuracy of 100% was achieved by extracting discriminative features from the same population that was used for testing the accuracy. To have more robust classification scheme, future studies may use the selected features to discriminate patients with AD from healthy controls in another dataset. In addition, more effort is needed to propose algorithms for differentiation of normal, mild cognitive impairment (MCI), and AD, simultaneously. This can be done by developing analysis methodologies to extract features from rs-fMRI signals that are sufficiently sensitive to detecting small functional changes during AD and MCI. The population size of study should be larger in future studies by establishment of large population-based rs-fMRI databases to evaluate the variability and stability of large-scale networks in the general population. Another limitation is related to the calculation of edges using simple Pearson correlation coefficient which neglects the time dynamics of the rs-fMRI time series.

5. Conclusions

We applied the graph theoretical approach and the pattern recognition method on the resting state fMRI data to classify patients with Alzheimer's disease (AD) from the normal subjects. The proposed method detected accurately specific sets of brain graph measures that are informative to distinguish normal subjects from patients with AD. Informative graph measures were related to the brain cortical regions using edges and nodes and provided information about disrupted brain functional nodes. When applied to functional data from groups of normal subjects and patients with AD, we were able to identify AD induced causes to the weighted brain network. The proposed algorithm in this study classified patients with AD and normal subjects with accuracy of 100%. However, further investigations are required for validation in larger independent datasets before utilizing the proposed method in clinical applications.

Acknowledgment

This study was funded by the Children's Foundation Research Institute, Le Bonheur Children's Hospital, Memphis, TN.

Conflict of interest: None declared.

References

Ashburner J, Friston KJ. Nonlinear spatial normalization using basis functions. Hum Brain Mapp 1999;7:254–66.
Barrat A, Barthelemy M, Pastor-Satorras R, Vespignani A. The architecture of complex weighted networks. Proc Natl Acad Sci USA 2004;101:3747–52.
Bassett DS, Bullmore E, Verchinski BA, Mattay VS, Weinberger DR, Meyer-Lindenberg A. Hierarchical organization of human cortical networks in health and schizophrenia. J Neurosci 2008;28:9239–48.
Bassett DS, Bullmore ET. Human brain networks in health and disease. Curr Opin Neurol 2009;22:340.
Ben-Hur A, Weston J. A user's guide to support vector machines. Data mining techniques for the life sciences. Springer; 2010. p. 223–39.
Benjamini Y, Hochberg Y. Controlling the false discovery rate: a practical and powerful approach to multiple testing. J R Stat Soc B (Method) 1995;75:289–300.
Biswal B, Zerrin Yetkin F, Haughton VM, Hyde JS. Functional connectivity in the motor cortex of resting human brain using echo-planar mri. Magn Reson Med 1995;34:537–41.
Blennow K, de Leon MJ, Zetterberg H. Alzheimer's disease. Lancet 2006;368:387–403.
Blondel VD, Guillaume J-L, Lambiotte R, Lefebvre E. Fast unfolding of communities in large networks. J Stat Mech Theory E 2008;2008:P10008.
Brandes U. A faster algorithm for betweenness centrality. J Math Sociol 2001;25:163–77.
Brier MR, Thomas JB, Snyder AZ, Benzinger TL, Zhang D, Raichle ME, et al. Loss of intranetwork and internetwork resting state functional connections with Alzheimer's disease progression. J Neurosci 2012;32:8890–9.
Bullmore E, Sporns O. Complex brain networks: graph theoretical analysis of structural and functional systems. Nat Rev Neurosci 2009;10:186–98.
Busatto GF, Garrido GE, Almeida OP, Castro CC, Camargo CH, Cid CG, et al. A voxel-based morphometry study of temporal lobe gray matter reductions in Alzheimer's disease. Neurobiol Aging 2003;24:221–31.
Chao-Gan Y, Yu-Feng Z. DPARSF: A MATLAB Toolbox for "Pipeline" Data Analysis of Resting-State fMRI. Front Syst Neurosci 2010;4:13.
Chen G, Ward BD, Xie C, Li W, Wu Z, Jones JL, et al. Classification of Alzheimer disease, mild cognitive impairment, and normal cognitive status with large-scale network analysis based on resting-state functional MR imaging. Radiology 2011;259:213.
Dai Z, Yan C, Wang Z, Wang J, Xia M, Li K, et al. Discriminative analysis of early Alzheimer's disease using multi-modal imaging and multi-level characterization with multi-classifier (M3). Neuroimage 2012;59:2187–95.
Desgranges B, Baron J-C, Giffard B, Chételat G, Lalevée C, Viader F, et al. The neural basis of intrusions in free recall and cued recall: a PET study in Alzheimer's disease. Neuroimage 2002;17:1658–64.
Dimitriadis SI, Laskaris NA, Tzelepi A, Economou G. Analyzing functional brain connectivity by means of commute times: a new approach and its application to track event-related dynamics. IEEE T Bio-Med Eng 2012;59:1302–9.
Duda RO, Hart PE, Stork DG. Pattern classification. John Wiley & Sons; 2012.
Eustache F, Piolino P, Giffard B, Viader F, De La Sayette V, Baron JC, et al. 'In the course of time': a PET study of the cerebral substrates of autobiographical amnesia in Alzheimer's disease. Brain 2004;127:1549–60.

Fox MD, Snyder AZ, Vincent JL, Corbetta M, Van Essen DC, Raichle ME. The human brain is intrinsically organized into dynamic, anticorrelated functional networks. Proc Natl Acad Sci USA 2005;102:9673–8.
Fransson P. Spontaneous low-frequency BOLD signal fluctuations: an fMRI investigation of the resting-state default mode of brain function hypothesis. Hum Brain Mapp 2005;26:15–29.
Freeman LC. Centrality in social networks conceptual clarification. Social Networks 1979;1:215–39.
Frisoni G, Testa C, Zorzan A, Sabattoli F, Beltramello A, Soininen H, et al. Detection of grey matter loss in mild Alzheimer's disease with voxel based morphometry. J Neurol Neurosurg Psychiatry 2002;73:657–64.
Friston KJ, Frith CD, Frackowiak RS, Turner R. Characterizing dynamic brain responses with fMRI: a multivariate approach. Neuroimage 1995;2:166–72.
Greicius MD, Krasnow B, Reiss AL, Menon V. Functional connectivity in the resting brain: a network analysis of the default mode hypothesis. Proc Natl Acad Sci 2003;100:253–8.
Greicius MD, Srivastava G, Reiss AL, Menon V. Default-mode network activity distinguishes Alzheimer's disease from healthy aging: evidence from functional MRI. Proc Natl Acad Sci USA 2004;101:4637–42.
Guimera R, Amaral LAN. Cartography of complex networks: modules and universal roles. J Stat Mech-Theory E 2005;2005:P02001.
Guimera R, Sales-Pardo M, Amaral LA. Classes of complex networks defined by role-to-role connectivity profiles. Nat Phys 2007;3:63–9.
He Y, Chen Z, Evans A. Structural insights into aberrant topological patterns of large-scale cortical networks in Alzheimer's disease. J Neurosci 2008;28:4756–66.
Hoekzema E, Carmona S, Ramos-Quiroga JA, Richarte Fernandez V, Bosch R, Soliva JC, et al. An independent components and functional connectivity analysis of resting state fMRI data points to neural network dysregulation in adult ADHD. Hum Brain Mapp 2014;35:1261–72.
Holtzman DM, Morris JC, Goate AM. Alzheimer's disease: the challenge of the second century. Sci Transl Med 2011;3:77sr1.
Humphries MD, Gurney K. Network 'small-world-ness': a quantitative method for determining canonical network equivalence. PLoS ONE 2008;3:e0002051.
Jack CR, Bernstein MA, Fox NC, Thompson P, Alexander G, Harvey D, et al. The Alzheimer's disease neuroimaging initiative (ADNI): MRI methods. J Magn Reson Imaging 2008;27:685–91.
Karas G, Scheltens P, Rombouts S, Visser P, Van Schijndel R, Fox N, et al. Global and local gray matter loss in mild cognitive impairment and Alzheimer's disease. Neuroimage 2004;23:708–16.
Kelly A, Uddin LQ, Biswal BB, Castellanos FX, Milham MP. Competition between functional brain networks mediates behavioral variability. Neuroimage 2008;39:527–37.
Kim S, Youn YC, Hsiung GY, Ha SY, Park KY, et al. Voxel-based morphometric study of brain volume changes in patients with Alzheimer's disease assessed according to the Clinical Dementia Rating score. J Clin Neurosci 2011;18:916–21.
Koch W, Teipel S, Mueller S, Benninghoff J, Wagner M, Bokde AL, et al. Diagnostic power of default mode network resting state fMRI in the detection of Alzheimer's disease. Neurobiol Aging 2012;33:466–78.
Latora V, Marchiori M. Efficient behavior of small-world networks. Phys Rev Lett 2001;87:198701.
Lee M, Smyser C, Shimony J. Resting-state fMRI: a review of methods and clinical applications. Am J Neuroradiol 2013;34:1866–72.
Li Y, Qin Y, Chen X, Li W. Exploring the functional brain network of Alzheimer's disease: based on the computational experiment. PLoS ONE 2013;8:e73186.
Liu F, Guo W, Fouche J-P, Wang Y, Wang W, Ding J, et al. Multivariate classification of social anxiety disorder using whole brain functional connectivity. Brain Struct Funct 2015;220:1–15.
Lo C-Y, Wang P-N, Chou K-H, Wang J, He Y, Lin C-P. Diffusion tensor tractography reveals abnormal topological organization in structural cortical networks in Alzheimer's disease. J Neurosci 2010;30:16876–85.
Lu H, Zuo Y, Gu H, Waltz JA, Zhan W, Scholl CA, et al. Synchronized delta oscillations correlate with the resting-state functional MRI signal. Proc Natl Acad Sci 2007;104:18265–9.
Lynall M-E, Bassett DS, Kerwin R, McKenna PJ, Kitzbichler M, Muller U, et al. Functional connectivity and brain networks in schizophrenia. J Neurosci 2010;30:9477–87.
Melrose RJ, Campa OM, Harwood DG, Osato S, Mandelkern MA, Sultzer DL. The neural correlates of naming and fluency deficits in Alzheimer's disease: an FDG-PET study. Int J Geriatr Psychiatry 2009;24:885–93.
Minoshima S, Giordani B, Berent S, Frey KA, Foster NL, Kuhl DE. Metabolic reduction in the posterior cingulate cortex in very early Alzheimer's disease. Ann Neurol 1997;42:85–94.
Noble WS. What is a support vector machine? Nat Biotechnol 2006;24:1565–7.
Onnela J-P, Saramäki J, Kertész J, Kaski K. Intensity and coherence of motifs in weighted complex networks. Phys Rev E 2005;71:065103.
Passingham RE, Stephan KE, Kötter R. The anatomical basis of functional localization in the cortex. Nat Rev Neurosci 2002;3:606–16.
Raichle ME, MacLeod AM, Snyder AZ, Powers WJ, Gusnard DA, Shulman GL. A default mode of brain function. Proc Natl Acad Sci 2001;98:676–82.
Reitz C, Brayne C, Mayeux R. Epidemiology of Alzheimer disease. Nat Rev Neurol 2011;7:137–52.
Rubinov M, Sporns O. Complex network measures of brain connectivity: uses and interpretations. Neuroimage 2010;52:1059–69.
Rubinov M, Sporns O. Weight-conserving characterization of complex functional brain networks. Neuroimage 2011;56:2068–79.
Sanz-Arigita EJ, Schoonheim MM, Damoiseaux JS, Rombouts SA, Maris E, Barkhof F, et al. Loss of 'small-world' networks in Alzheimer's disease: graph analysis of FMRI resting-state functional connectivity. PLoS ONE 2010;5:e13788.
Schölkopf B, Tsuda K, Vert J-P. Kernel methods in computational biology. MIT press.
Smith GS, Kramer E, Ma Y, Hermann CR, Dhawan V, Chaly T, et al. Cholinergic modulation of the cerebral metabolic response to citalopram in Alzheimer's disease. Brain 2009;132:392–401.
Sorg C, Riedl V, Mühlau M, Calhoun VD, Eichele T, Läer L, et al. Selective changes of resting-state networks in individuals at risk for Alzheimer's disease. Proc Natl Acad Sci 2007;104:18760–5.
Sporns O, Honey CJ. Small worlds inside big brains. Proc Natl Acad Sci 2006;103:19219–20.
Sporns O, Tononi G, Kötter R. The human connectome: a structural description of the human brain. PLoS Comput Biol 2005;1:e42.
Stam C, Jones B, Nolte G, Breakspear M, Scheltens P. Small-world networks and functional connectivity in Alzheimer's disease. Cereb Cortex 2007;17:92–9.
Tang Y, Jiang W, Liao J, Wang W, Luo A. Identifying individuals with antisocial personality disorder using resting-state FMRI. PLoS ONE 2013;8:e60652.
Theiler J, Eubank S, Longtin A, Galdrikian B, Doyne Farmer J. Testing for nonlinearity in time series: the method of surrogate data. Physica D 1992;58:77–94.
Tijms BM, Wink AM, de Haan W, van der Flier WM, Stam CJ, Scheltens P, et al. Alzheimer's disease: connecting findings from graph theoretical studies of brain networks. Neurobiol Aging 2013;34:2023–36.
Tzourio-Mazoyer N, Landeau B, Papathanassiou D, Crivello F, Etard O, Delcroix N, et al. Automated anatomical labeling of activations in SPM using a macroscopic anatomical parcellation of the MNI MRI single-subject brain. Neuroimage 2002;15:273–89.
van den Heuvel MP, Mandl RC, Stam CJ, Kahn RS, Pol HEH. Aberrant frontal and temporal complex network structure in schizophrenia: a graph theoretical analysis. J Neurosci 2010;30:15915–26.
Wang K, Jiang T, Liang M, Wang L, Tian L, Zhang X, et al. Discriminative analysis of early Alzheimer's disease based on two intrinsically anti-correlated networks with resting-state fMRI. Medical Image Computing and Computer-Assisted Intervention – MICCAI 2006. Springer; 2006. p. 340–7.
Wang K, Liang M, Wang L, Tian L, Zhang X, Li K, et al. Altered functional connectivity in early Alzheimer's disease: a resting-state fMRI study. Hum Brain Mapp 2007;28:967–78.
Wang L, Metzak PD, Honer WG, Woodward TS. Impaired efficiency of functional networks underlying episodic memory-for-context in schizophrenia. J Neurosci 2010;30:13171–9.
Wang L, Zang Y, He Y, Liang M, Zhang X, Tian L, et al. Changes in hippocampal connectivity in the early stages of Alzheimer's disease: evidence from resting state fMRI. Neuroimage 2006b;31:496–504.
Watts DJ, Strogatz SH. Collective dynamics of 'small-world' networks. Nature 1998;393:440–2.
Zeng LL, Shen H, Liu L, Hu D. Unsupervised classification of major depression using functional connectivity MRI. Hum Brain Mapp 2014;35:1630–41.
Zhang J, Wang J, Wu Q, Kuang W, Huang X, He Y, et al. Disrupted brain connectivity networks in drug-naive, first-episode major depressive disorder. Biol Psychiatry 2011;70:334–42.
Zhang Z, Liu Y, Jiang T, Zhou B, An N, Dai H, et al. Altered spontaneous activity in Alzheimer's disease and mild cognitive impairment revealed by Regional Homogeneity. Neuroimage 2012;59:1429–40.